

Article

A Novel Inherently Flame-Retardant Composite Based on Zinc Alginate/Nano-Cu₂O

Peng Xu ¹, Peiyuan Shao ¹, Qing Zhang ¹, Wen Cheng ¹, Zichao Li ^{2,*}  and Qun Li ^{1,*} 

¹ College of Chemical Science and Engineering, Qingdao University, Qingdao 266071, China; X1627271005@163.com (P.X.); 2017020828@qdu.edu.cn (P.S.); 20180205203@qdu.edu.cn (Q.Z.); wencheney2014@163.com (W.C.)

² Institute of Advanced Cross-Field Science, College of Life Sciences, Qingdao University, Qingdao 266071, China

* Correspondence: qunli@qdu.edu.cn (Q.L.); zichao.li@qdu.edu.cn (Z.L.); Tel.: +86-532-8595-0705 (Q.L.)

Received: 31 August 2019; Accepted: 25 September 2019; Published: 27 September 2019



Abstract: A novel flame-retardant composite material based on zinc alginate (ZnAlg) and nano-cuprous oxide (Cu₂O) was prepared through a simple, eco-friendly freeze-drying process and a sol-gel method. The composites were characterized and their combustion and flammability behavior were tested. The composites had high thermal stability and achieved nearly non-flammability with a limiting oxygen index (LOI) of 58. The results show remarkable improvement of flame-retardant properties in the ZnAlg/Cu₂O composites, compared to ZnAlg. Furthermore, the pyrolysis behavior was determined by pyrolysis–gas chromatography–mass spectrometry (Py-GC-MS) and the flame-retardant mechanism was proposed based on the combined experimental results. The prepared composites show promising application prospects in building materials and the textile industry.

Keywords: zinc alginate; nano-Cu₂O; flame retardancy; pyrolysis; thermal degradation

1. Introduction

Sodium alginate (NaAlg) is a hydrophilic and biodegradable linear polysaccharide copolymer consisting of two different ratios of spatially different 1,4-linked α -L guluronic acid and β -D mannuronic acid repeating unit composition [1–3]. The unique properties of sodium alginate are biological origin, non-toxic, hydrophilic, biocompatible, biodegradable and low-cost, making it highly applicable in various fields [4,5]. The most important characteristic of NaAlg is that it can react with polyvalent metal cations to form strong gels or insoluble polymers [6–8], thereby improving water resistance, mechanical properties, barrier properties, cohesiveness and rigidity during cross-linking with multivalent cations [9]. Zinc alginate is a material with excellent biological activity and is widely used in flame-retardant and antibacterial applications [10,11].

Nanomaterials have a wide range of applications in flame retardancy [12]. Norouzi et al. investigated the effect of the addition of different nanomaterials on the flame retardancy of textiles and found that most nanoparticles can improve the thermal stability and flame-resistant textile polymers [13]. Nanoparticles of different kinds of materials, such as silver, titanium dioxide and zinc oxide, have been reported to be functionalized for fibers and fabrics to achieve significantly improved products with new macroscopic properties [14]. Nano-Cu₂O is a new type of p-type oxide semiconductor material that can be excited by visible light. It has an active electron-hole pair system and exhibits good catalytic activities [15–17]. In addition, it shows excellent adsorption properties and low-temperature paramagnetism, and has potential applications in organic synthesis, photoelectric conversion, new energy, photolysis of water, dye bleaching, sterilization, superconductivity and other

fields [17–23]. However, few studies have been focused on flame retardancy of materials based on nano-Cu₂O to date.

In this study, ZnAlg/Cu₂O composite materials were prepared by a simple, economical and environmentally friendly sol-gel method. The composites were characterized by scanning electron microscopy (SEM), X-ray diffractometry (XRD), X-ray photoelectron spectroscopy (XPS), Fourier transform infrared spectrum (FTIR), and thermogravimetric analysis (TG). The combustion and flammability behaviors of the composites were assessed by the limiting oxygen index (LOI), vertical burning rate (UL-94) and cone calorimetry (CONE). Additionally, the pyrolysis products of the composites, SEM of the char residue, were investigated to reveal the flame-retardant mechanism of the prepared materials.

2. Materials and Methods

2.1. Materials

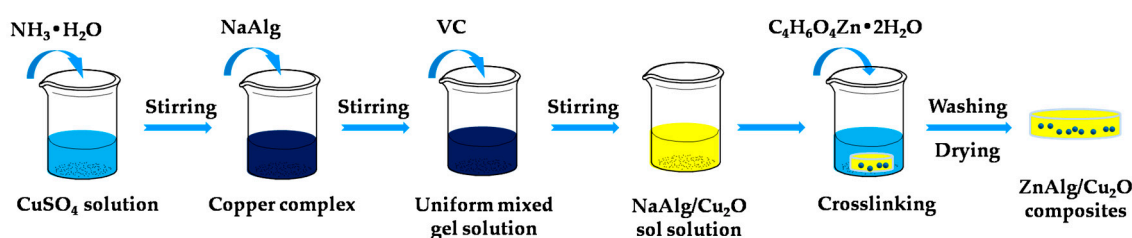
NaAlg was supplied by the Institute of Photosynthetic Fine Chemicals (Tianjin, China). Cupric sulfate (CuSO₄·5H₂O) was purchased from Tianjin Beichen Founder Reagent Factory (Tianjin, China). Zinc acetate dehydrate (C₄H₆O₄Zn·2H₂O) and L-Ascorbic acid (VC) were obtained from Sinopharm Chemical Reagent Co., Ltd. (Shanghai, China). Ammonia solution (NH₃·H₂O) was purchased from Kant Chemical Co., Ltd. (Laiyang, China). All the chemicals were not further purified and all the solutions were prepared using deionized water.

2.2. Preparation of ZnAlg

Firstly, 20.00 g of NaAlg was added in 500 mL deionized water and stirred to form a uniform sol. After standing for 24 h, the NaAlg sol was shaped in a square mold. Then, 3 wt % C₄H₆O₄Zn·2H₂O solution was added and crosslinked with NaAlg for 48 h. The final product was washed several times with deionized water and dried in a freeze dryer (FD-1A-50, Billing Instrument Manufacturing Co., Ltd, Shanghai, China).

2.3. Preparation of ZnAlg/Cu₂O Composites

The ZnAlg/Cu₂O composites were prepared as illustrated in Scheme 1. Briefly, CuSO₄·5H₂O (2.34 g) was dissolved in 450 mL deionized water and stirred to uniform dispersion in deionized water. Then, 7.5 mL of NH₃·H₂O was added and stirred to form a copper complex solution. Subsequently, 20.00 g of NaAlg was slowly added and stirred to form a uniform mixed gel solution. After standing for 24 h, 50 mL 13.67 wt % VC solution was slowly added to the mixed gel solution and stirred until it turned yellow to produce the NaAlg/Cu₂O mixed gel solution. The as-prepared gel solution was poured and shaped in a square mold, followed by the addition of 3 wt % C₄H₆O₄Zn·2H₂O (500 mL) solution. Crosslinked reaction was proceeded for 24 h to obtain the ZnAlg/Cu₂O composites. The final product was washed several times with deionized water and dried in a freeze dryer for further use.



Scheme 1. Preparation of ZnAlg/Cu₂O composite materials.

2.4. Measurements

The morphology and microstructure of the samples were examined by SEM (SIGMA, Zeiss, Oberkochen, Germany). All samples on the surface of the study were sprayed with gold.

The XRD of the prepared sample was carried out on a D8 Advance diffractometer (Bruker, Karlsruhe, Germany). The sample was scanned in 2θ to 90° in continuous mode.

The XPS was recorded on an ESCALAB 250Xi (Thermo Fisher Scientific, Waltham, MA, USA). The orbit of Cu element is 2p orbital.

The chemical bonds in the samples were determined by FTIR spectroscopy (NICOLET iS50, Thermo Fisher Scientific, Madison, WI, USA). The wavenumbers ranged from 4000 to 500 cm^{-1} .

The LOI tests were performed on a digital limiting oxygen index tester (LFY-606B, Shandong Textile Science Research Institute, Jinan, China) according to the standard method ISO 4589-1:1996. The size of all samples was $130\text{ mm} \times 10\text{ mm}$.

The UL-94 tests were performed on a LFY-601A vertical burning rate tester (Shandong Textile Science Research Institute, Jinan, China) according to the standard method ANST/UL-94-1985. The size of all samples was $130\text{ mm} \times 13\text{ mm} \times 5\text{ mm}$.

TG was carried out on an SDT Q600 thermogravimetric analyzer (TA Instrument, New Castle, DE, USA), and the samples were raised from 25 to $900\text{ }^\circ\text{C}$ at a heating rate of $10\text{ }^\circ\text{C}/\text{min}$ in ambient environment as well as nitrogen atmosphere.

The combustion properties of the samples were measured using an FTT-0242 cone calorimeter device (Fire Testing Technology, East Grinstead, UK) under an external heat flux of $35\text{ kW}/\text{m}^2$ according to standard ISO 5660. The dimensions of all samples were $100\text{ mm} \times 100\text{ mm} \times 3\text{ mm}$.

Py-GC-MS was performed by a thermal cracker (EGA/PY-3030D, Frontier, Koriyama, Japan) and gas chromatography–mass spectrometer (TRACE 1310-ISQLT, Thermo Fisher Scientific, Waltham, MA, USA). The pyrolysis temperature was 250 , 450 , and $750\text{ }^\circ\text{C}$, and the carrier gas was He. The GC temperature program was started at $50\text{ }^\circ\text{C}$, and stayed in the pose for 3 min , and then rose to $300\text{ }^\circ\text{C}$ at the speed of $20\text{ }^\circ\text{C}/\text{min}$.

3. Results and Discussion

3.1. Characterizations

The morphology of the prepared samples was investigated by SEM and the images are shown in Figure 1. It can be observed from Figure 1a that the surface of ZnAlg showed a network structure and was relatively rough. As can be seen from Figure 1b, spherical nano- Cu_2O was embedded in ZnAlg, ranging from 100 – 400 nm in size, indicating a successful preparation of the ZnAlg/ Cu_2O composites. Moreover, the addition of nano- Cu_2O made the surface of ZnAlg smoother.

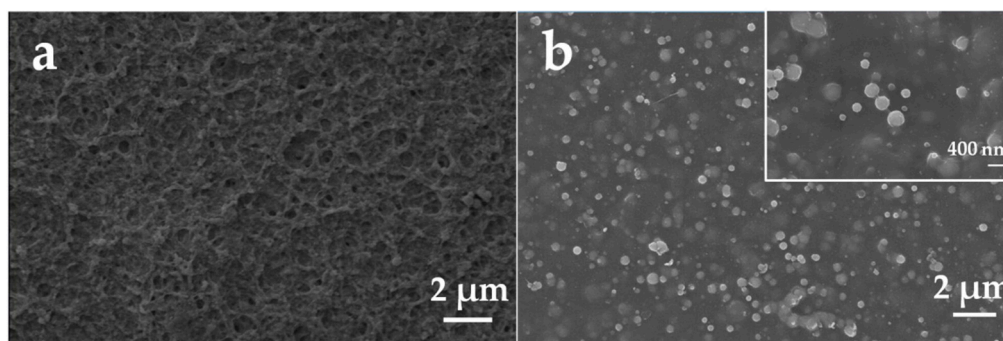


Figure 1. SEM images of (a) ZnAlg and (b) ZnAlg/ Cu_2O composites. The inset in (b) is its magnified image.

The diffraction peaks at 36.46° , 42.34° and 61.43° of the ZnAlg/ Cu_2O samples can be seen in Figure 2a, which can be assigned to Cu_2O , indicating a successful introduction of Cu_2O for the sample

preparation [24]. Moreover, no other obvious peaks can be observed in the images, suggesting high purity of Cu_2O in the material.

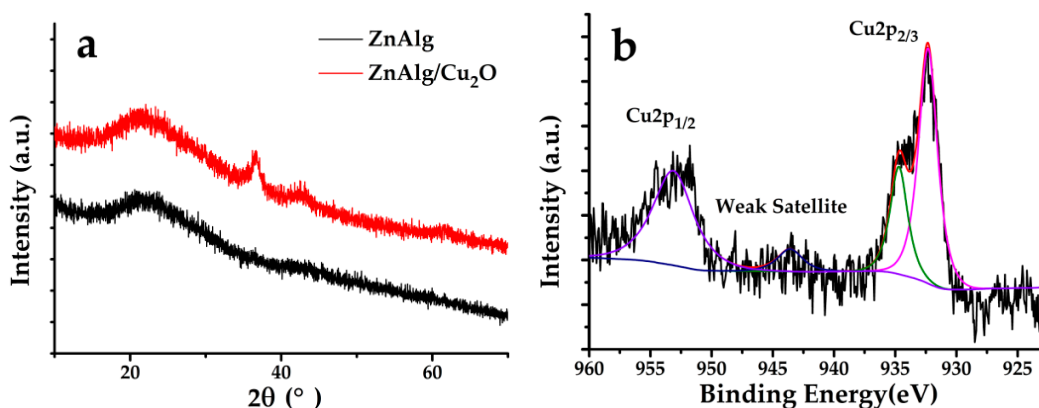


Figure 2. (a) X-ray diffractometry (XRD) patterns of ZnAlg and ZnAlg/ Cu_2O and (b) main and satellite peaks of Cu 2p_{3/2} and Cu 2p_{1/2} of the X-ray photoelectron spectroscopy (XPS) spectra for ZnAlg/ Cu_2O .

Figure 2b displays the XPS spectrum of the ZnAlg/ Cu_2O composites. As seen, the two peaks at 932.7 and 953.2 eV can be corresponded to the Cu 2p_{3/2} and Cu 2p_{1/2} binding energies of Cu_2O . The results reflect the high purity of Cu_2O in ZnAlg/ Cu_2O , which is in good agreement with that of previous reports [25–28]. Moreover, as shown in Figure S1 (in Supplementary Materials), the content of Cu was 0.75 at. %, while that of Zn was 2.17 at. %.

The FTIR spectra of the samples are shown in Figure 3. A series of characteristic absorption peaks were observed, of which 3240 cm^{-1} (O–H stretching vibration), 2923 cm^{-1} (– CH_2), 1584 cm^{-1} (C=O stretching vibration) [29], 1429 cm^{-1} (symmetric and asymmetric vibrations of –COO), 1029 and 914 cm^{-1} (symmetric and asymmetric vibrations of C–O–C), respectively. No significant differences between the infrared peaks of ZnAlg/ Cu_2O and ZnAlg can be noticed, indicating that the addition of Cu_2O did not break the structure of ZnAlg [30,31].

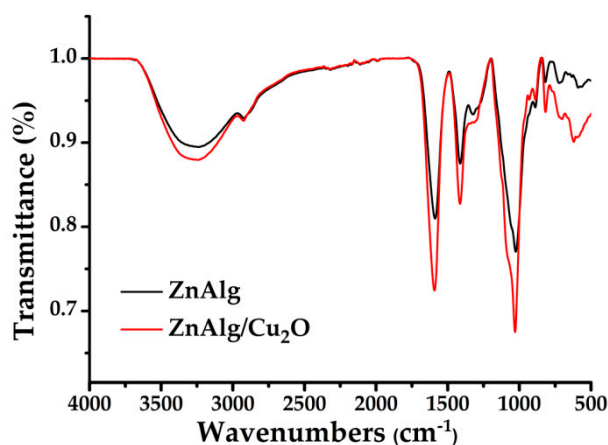


Figure 3. Fourier transform infrared spectrum (FTIR) spectra of ZnAlg and ZnAlg/ Cu_2O .

3.2. Thermal Stability

The thermal stability of the materials was tested in the air as well as the nitrogen atmosphere, and the results show both materials had similar degradation trends. It can be observed from Figure 4a,b that, under air, from the start of heating to $200\text{ }^\circ\text{C}$, there was about 18% weight loss, which was caused by evaporation of free water and crystal water in the materials, suggesting high natural moisture regain of the materials [31]. From 200 to $450\text{ }^\circ\text{C}$, the masses of ZnAlg/ Cu_2O and ZnAlg were dropped sharply, which was mainly due to the cleavage of glycosidic bonds in the alginate, as well as decarboxylation

and decarbonylation [32]. Over 450 °C, the mass of ZnAlg remained nearly unchanged, and the phase change mainly occurred during this period [8], while the mass of ZnAlg/Cu₂O increased, which was caused by the oxidation of Cu₂O to CuO ($2\text{Cu}_2\text{O} + \text{O}_2 = 4\text{CuO}$) [33,34]. The results show that ZnAlg/Cu₂O produced more residues than ZnAlg, which was about 6% higher, indicating better thermal stability of ZnAlg/Cu₂O [35,36].

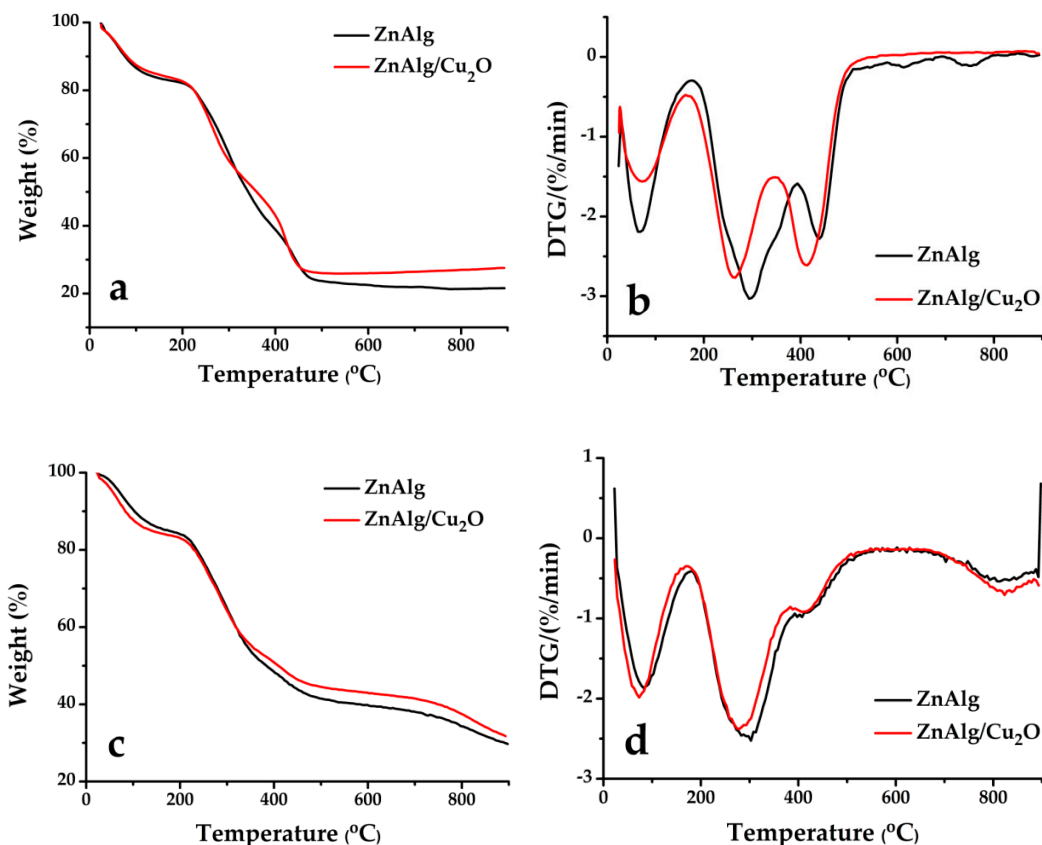


Figure 4. (a) Thermogravimetric analysis (TG) and (b) derivative thermogravimetry (DTG) curves of ZnAlg/Cu₂O and ZnAlg under air; (c) TG and (d) DTG curves of ZnAlg/Cu₂O and ZnAlg under nitrogen.

In nitrogen atmosphere, displayed in Figure 4c,d, from the beginning to 200 °C, the ZnAlg curve ran above the ZnAlg/Cu₂O curve, indicating that the natural moisture regain of ZnAlg/Cu₂O was higher, and the addition of Cu₂O accelerated the dehydration of ZnAlg. At 200–300 °C, ZnAlg and ZnAlg/Cu₂O almost lost weight simultaneously, suggesting that Cu₂O did not play its part within this period. After 450 °C, the mass of ZnAlg/Cu₂O continued to decrease in the nitrogen environment, while the mass of ZnAlg/Cu₂O increased under air, which further confirmed the oxidation of Cu₂O. The weight loss rate of ZnAlg/Cu₂O was significantly lower than that of ZnAlg, suggesting that O₂ can be absorbed during the oxidation of Cu₂O to CuO, thereby suppressing combustion [35]. It can be inferred that CuO can act as dust on ZnAlg, to absorb heat and dissipate in the combustion area, thus inhibited the degradation of ZnAlg [31].

3.3. Flame Retardancy

The flame-retardant properties of the two prepared samples were investigated by LOI and UL-94 tests and the test data are listed in Table 1. As seen, both ZnAlg/Cu₂O and ZnAlg had a high LOI. Moreover, the LOI of ZnAlg was increased from 49 to 58, indicating that the introduction of Cu₂O can efficiently improve the flame retardancy of the basic material. ZnAlg/Cu₂O was extinguished within 10 s after being ignited in the vertical burning test, and it passed the test without any dripping, which is favorable for its further real application.

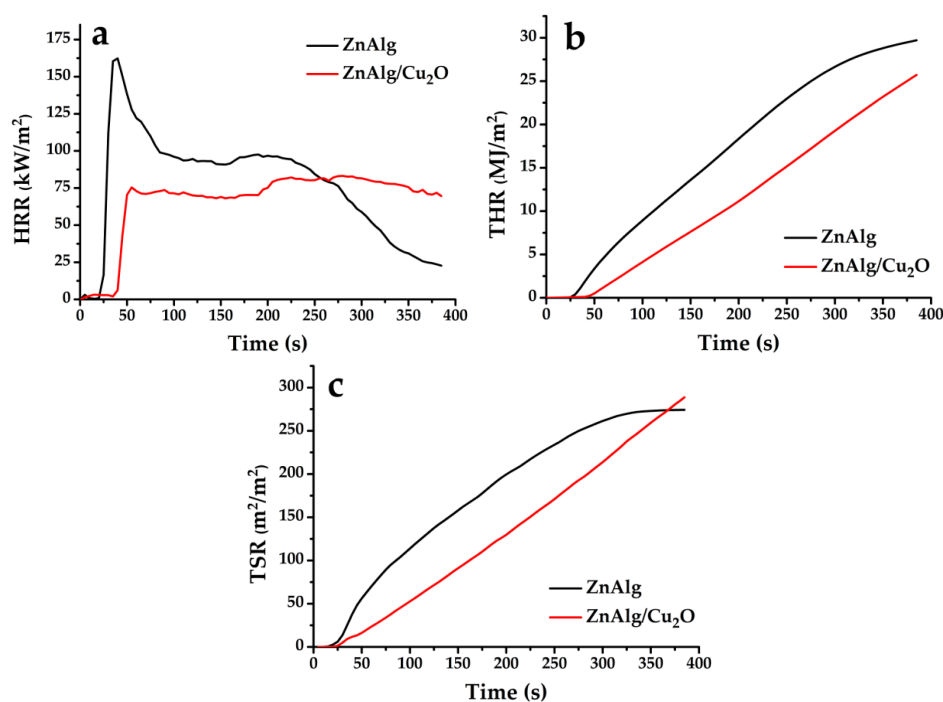
Table 1. Limiting oxygen index (LOI), vertical burning rate (UL-94) testing results and combustion parameters of the prepared samples.

Sample	LOI (%)	UL-94	Time to Ignition (s)	Time to Flameout (s)	THR (MJ/m ²)	PHRR (kW/m ²)	TSR (m ² /m ²)	Residue (%)
ZnAlg	49	V-0	22	387	29.71	162.31	274.28	51.29
ZnAlg/Cu ₂ O	58	V-0	37	610	25.71	83.18	288.75	56.74

PHRR: peak heat release rate; THR: total heat release; TSR: total smoke release.

3.4. Combustion Behavior

CONE has been widely employed to evaluate the combustion behavior of the polymers [37,38]. The most important flame-retardant parameters that CONE can give out are ignition time, heat release rate (HRR) and total heat release (THR), as these parameters may be related to flame growth and toxic gas emissions during combustion [1,39]. The detailed data are collected in Table 1 and the related curves are displayed in Figure 5. The ignition time of ZnAlg was 22 s, while that of ZnAlg/Cu₂O was 37 s, indicating that the polymers were more difficult to be burnt. HRR is an important parameter for evaluating fire safety [40,41]. As shown in Figure 5a, the HRR value of ZnAlg/Cu₂O was much lower than that of ZnAlg in the most part of the combustion processes. Moreover, the peak heat release rate (PHRR) of ZnAlg/Cu₂O was only 83.18 kW/m², compared to that of ZnAlg which was 162.31 kW/m². As seen in Table 1, ZnAlg was burnt completely at 387 s, while ZnAlg/Cu₂O continued and completed at 610 s, indicating that ZnAlg was more easily flammable than ZnAlg/Cu₂O, and that the catalytic and carbon formation function of Cu₂O reduced the combustion properties of the material. It can be observed from Figure 5b,c that the THR and TSR values of the two samples were increased with time. ZnAlg/Cu₂O showed lower THR and TSR values, suggesting lower heat release and less smoke release than ZnAlg. This may be attributed to the fact that O₂ can be absorbed during the oxidation process of Cu₂O to CuO at high temperatures. The generated CuO can act as a dust layer on the ZnAlg, absorbing heat in the combustion zone and blocking the release of smoke. In addition, the residual amount of ZnAlg/Cu₂O was higher than that of ZnAlg. Combining these results, the ZnAlg/Cu₂O composites showed remarkably better flame retardancy than ZnAlg.

**Figure 5.** (a) HRR, (b) THR and (c) TSR curves of ZnAlg and ZnAlg/Cu₂O changing with time.

3.5. Flame-Retardant Mechanism

Py-GC-MS is mainly used to analyze the main components of gaseous products produced during the pyrolysis of materials [42]. The chromatograms of ZnAlg/Cu₂O obtained by Py-GC-MS at 250, 450 and 750 °C are shown in Figure 6, respectively, and the major pyrolysis products determined by comparison with the NIST library are listed in Table 2. The main compounds produced at 450 °C were CO₂, CO, furfural, acetic acid, propanoic acid, 2-oxo-, n-hexadecanoic acid and 9-hexadecenoic acid. As can be seen, the main products can be divided into four groups, including CO, CO₂, organic acids and aldehydes, respectively [43]. As the temperature increased, more aromatic hydrocarbons, alcohols and ketones were produced. Figure S2 (in Supplementary Materials) displays the chromatograms of ZnAlg obtained by Py-GC-MS at 750 °C, and the main pyrolysis products identified based on the comparison with the NIST library are listed in Table S1 (in Supplementary Materials). Compared with ZnAlg, ZnAlg/Cu₂O produced less compounds, indicating that the addition of Cu₂O increased the char yield of ZnAlg. The formed carbon layer covered the surface of the matrix material, hindering the heat transfer and exchange of combustible gases between the matrix material and the outside. It had well protective function to the matrix material, thereby can improve its thermal stability [30,31].

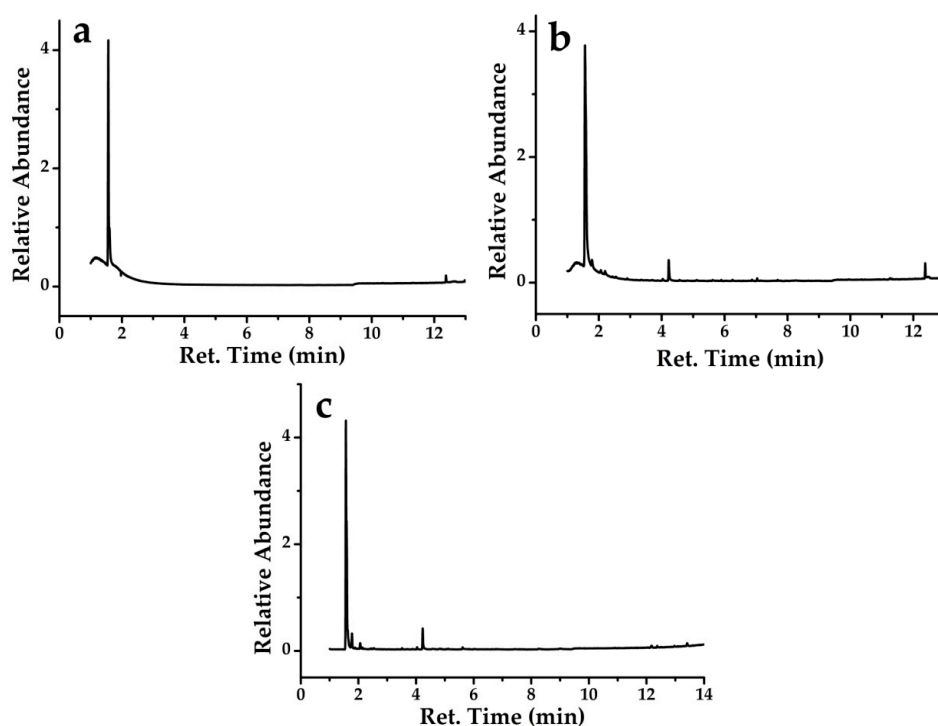


Figure 6. Py-GC-MS spectra of ZnAlg/Cu₂O at 250 °C (a), 450 °C (b) and 750 °C (c).

Table 2. Pyrolysis products of ZnAlg/Cu₂O at different temperatures.

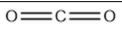
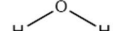

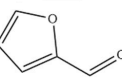
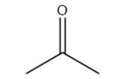
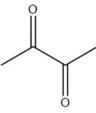
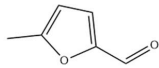
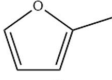
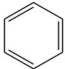
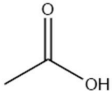
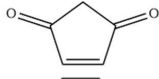

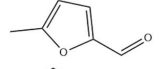
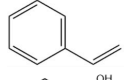
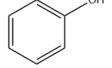
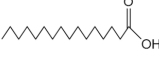
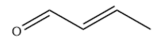
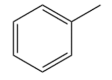
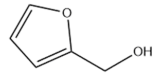
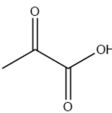
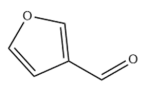
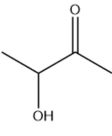
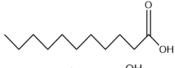
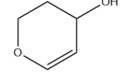

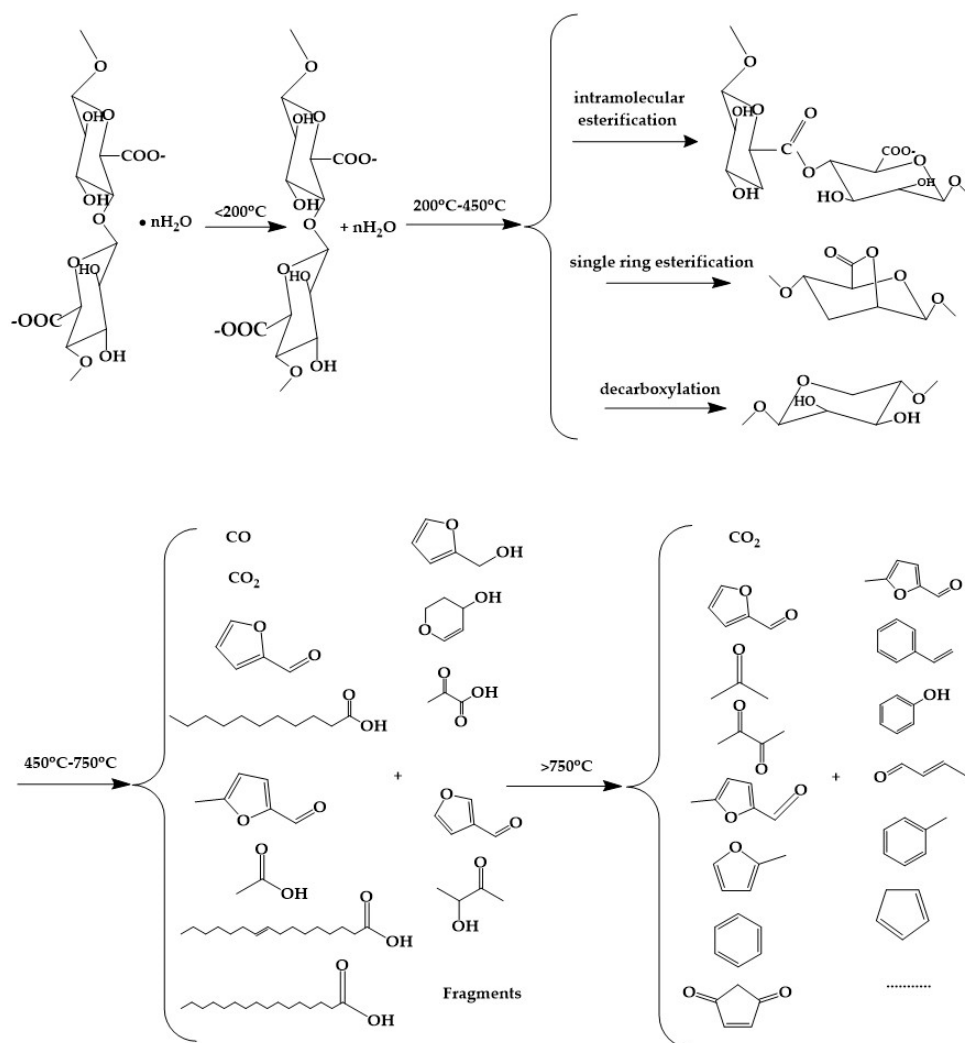
Molecular Structure Name of Compound	T = 250 °C		T = 450 °C		T = 750 °C	
	Time	Area	Time	Area	Time	Area
 carbon dioxide	1.87	2.03	1.57	71.37	1.57	74.46
 water	1.57	68.52	-	-	-	-
 carbon monoxide	1.15	18.36	1.26	6.74	-	-
 furfural	-	-	4.23	3.88	4.23	5.67
 acetone	-	-	-	-	1.78	3.54

Table 2. Cont.

Molecular Structure	Name of Compound	T = 250 °C		T = 450 °C		T = 750 °C	
		Time	Area	Time	Area	Time	Area
	2,3-butanedione	-	-	-	-	2.06	1.24
	2-furancarboxaldehyde,5-methyl	-	-	5.62	0.27	5.62	0.74
	furan,2-methyl-	-	-	-	-	2.14	0.30
	benzene	-	-	-	-	2.53	0.50
	acetic acid	-	-	2.20	1.03	-	-
	4-cyclopentene-1,3-dione	-	-	-	-	4.83	0.37
	1,3-cyclopentadiene	-	-	-	-	1.89	0.14
	2-furancarboxaldehyde,5-methyl	-	-	-	-	5.12	0.73
	styrene	-	-	-	-	4.90	0.12
	phenol	-	-	-	-	6.04	0.19
	n-hexadecanoic acid	12.38	1.68	12.38	2.25	-	-
	2-butenal, (E)-	-	-	-	-	2.44	0.27
	toluene	-	-	-	-	3.51	0.34
	2-furanmethanol	-	-	7.03	0.46	-	-
	propanoic acid, 2-oxo-	-	-	1.79	1.33	-	-
	3-furaldehyde	-	-	4.03	0.48	-	-
	acetoin	-	-	2.91	0.23	-	-
	undecanoic acid	-	-	8.26	0.29	-	-
	2h-pyran, 3,4-dihydro-4-hydroxy	-	-	11.26	0.30	-	-
	9-hexadecenoic acid	-	-	9.60	0.91	-	-

According to the test results of Py-GC-MS, the proposed thermal degradation mechanisms of ZnAlg/Cu₂O are depicted in Scheme 2. Below 200 °C, the decomposition products of the composites contained a large amount of H₂O, indicating massive loss of free and bound water. From 200 to 450 °C, the glycosidic bond of ZnAlg/Cu₂O was broken, while esterification and decarboxylation reaction occurred. Furthermore, as the degradation mechanism is complicated, thus an intramolecular esterification process (or between different rings) can more likely occur during the process and contribute to the cross-linking of the organic material to form carbon layers [44,45]. From 450 to 750 °C, dehydroxylation, decarboxylation, esterification, decarbonylation, rupture and rearrangement were believed to contribute to the improvement of char formation, releasing CO₂, CO, organic acids and aldehydes, such as furfural, acetic acid, propanoic acid, 2-oxo-, n-hexadecanoic acid, 9-hexadecenoic acid and etc. The above chemical reactions may be catalyzed by CuO. At 750 °C, the residue may be further degraded by condensation reaction. Cu₂O accelerated the dehydration of ZnAlg at low temperatures, which caused the formation of a carbon barrier. Furthermore, O₂ can be absorbed during the Cu₂O oxidation to CuO at high temperatures. The generated CuO can act as dust covered on ZnAlg, absorbing heat and dissipating in the combustion zone. According to the theory of wall effect, the flame cannot grow if dust is sufficient in the air [46]. Therefore, it can be inferred from the combined results that the introduction of Cu₂O to ZnAlg significantly improved its flame retardancy.



Scheme 2. Proposed thermal degradation mechanism of ZnAlg/Cu₂O.

4. Conclusions

A new intrinsic flame-retardant composite based on ZnAlg/nano-Cu₂O was first prepared through a simple, economical and environmentally friendly method. The prepared material exhibited excellent flame-retardant properties. It was found that the addition of nano-Cu₂O can promote the conversion of ZnAlg to carbon-based materials. Moreover, O₂ can be absorbed during the oxidation of Cu₂O to CuO at high temperatures. The CuO in the polymer can act as dust on the substrate material, covering on its surface when burnt. Thus, it can hinder the heat transfer between the matrix material and the outside and provided good protection on the matrix material. Therefore, the prepared materials can be highly prospective for application in building insulation materials and textile industry.

Supplementary Materials: The following are available online at <http://www.mdpi.com/2073-4360/11/10/1575/s1>, Figure S1: The XPS spectra of survey for ZnAlg/Cu₂O; Figure S2: Py-GC-MS spectra of ZnAlg at 750 °C; Table S1: Pyrolysis products of ZnAlg at 750 °C.

Author Contributions: Q.L. and Z.L. conceived and designed the experiments; P.X. and P.S. performed the experiments; Q.Z., W.C., Z.L. and Q.L. analyzed the data; P.X. and Z.L. wrote the paper.

Funding: This work was supported by the National Natural Science Foundation of China (grant number 51773102).

Conflicts of Interest: The authors declare no conflict of interest.

References

1. Zhang, J.; Ji, Q.; Shen, X.; Xia, Y.; Tan, L.; Kong, Q. Pyrolysis products and thermal degradation mechanism of intrinsically flame-retardant calcium alginate fibre. *Polym. Degrad. Stab.* **2011**, *96*, 936–942. [[CrossRef](#)]
2. Wang, L.; Shelton, R.; Cooper, P.; Lawson, M.; Triffitt, J.; Barralet, J. Evaluation of sodium alginate for bone marrow cell tissue engineering. *Biomaterials* **2003**, *24*, 3475–3481. [[CrossRef](#)]
3. Motwani, S.K.; Chopra, S.; Talegaonkar, S.; Kohl, K.; Ahmad, F.J.; Khar, R.K. Chitosan-sodium alginate nanoparticles as submicroscopic reservoirs for ocular delivery: Formulation, optimisation and in vitro characterisation. *Eur. J. Pharm. Biopharm.* **2008**, *68*, 513–525. [[CrossRef](#)] [[PubMed](#)]
4. Rhim, J.-W. Physical and mechanical properties of water resistant sodium alginate films. *LWT-Food Sci. Technol.* **2004**, *37*, 323–330. [[CrossRef](#)]
5. Shalumon, K.; Anulekha, K.; Nair, S.V.; Nair, S.; Chennazhi, K.P.; Jayakumar, R. Sodium alginate/poly (vinyl alcohol)/nano ZnO composite nanofibers for antibacterial wound dressings. *Int. J. Boil. Macromol.* **2011**, *49*, 247–254. [[CrossRef](#)] [[PubMed](#)]
6. Liu, Y.; Zhao, J.C.; Zhang, C.J.; Guo, Y.; Zhu, P.; Wang, D.Y. Effect of manganese and cobalt ions on flame retardancy and thermal degradation of bio-based alginate films. *J. Mater. Sci.* **2016**, *51*, 1052–1065. [[CrossRef](#)]
7. Kong, Q.-S.; Wang, B.-B.; Ji, Q.; Xia, Y.-Z.; Guo, Z.-X.; Yu, J. thermal degradation and flame retardancy of calcium alginate fibers. *Chin. J. Polym. Sci.* **2009**, *27*, 807. [[CrossRef](#)]
8. Liu, Y.; Zhao, J.; Zhang, C.; Ji, H.; Zhu, P. The Flame Retardancy, Thermal Properties, and Degradation Mechanism of Zinc Alginate Films. *J. Macromol. Sci. Part B* **2014**, *53*, 1074–1089. [[CrossRef](#)]
9. Zhang, J.; Ji, Q.; Wang, F.; Tan, L.; Xia, Y. Effects of divalent metal ions on the flame retardancy and pyrolysis products of alginate fibres. *Polym. Degrad. Stab.* **2012**, *97*, 1034–1040. [[CrossRef](#)]
10. Chan, L.; Jin, Y.; Heng, P. Cross-linking mechanisms of calcium and zinc in production of alginate microspheres. *Int. J. Pharm.* **2002**, *242*, 255–258. [[CrossRef](#)]
11. Straccia, M.C.; D’Ayala, G.G.; Romano, I.; Laurienzo, P. Novel zinc alginate hydrogels prepared by internal setting method with intrinsic antibacterial activity. *Carbohydr. Polym.* **2015**, *125*, 103–112. [[CrossRef](#)] [[PubMed](#)]
12. Wang, Z.; Han, E.; Ke, W. Effect of nanoparticles on the improvement in fire-resistant and anti-ageing properties of flame-retardant coating. *Surf. Coat. Technol.* **2006**, *200*, 5706–5716. [[CrossRef](#)]
13. Norouzi, M.; Zare, Y.; Kiany, P. Nanoparticles as Effective Flame Retardants for Natural and Synthetic Textile Polymers: Application, Mechanism, and Optimization. *Polym. Rev.* **2015**, *55*, 531–560. [[CrossRef](#)]
14. Rivero, P.J.; Urrutia, A.; Goicoechea, J.; Arregui, F.J. Nanomaterials for Functional Textiles and Fibers. *Nanoscale Res. Lett.* **2015**, *10*, 501. [[CrossRef](#)] [[PubMed](#)]
15. Gou, L.; Murphy, C.J. Solution-Phase Synthesis of Cu₂O Nanocubes. *Nano Lett.* **2003**, *3*, 231–234. [[CrossRef](#)]

16. Li, C.L.; Li, Y.B.; Delaunay, J.J. A novel method to synthesize highly photoactive Cu₂O microcrystalline films for use in photoelectrochemical cells. *Acs Appl. Mater. Inter.* **2014**, *6*, 480–486. [[CrossRef](#)] [[PubMed](#)]
17. Pan, L.; Zou, J.J.; Zhang, T.R.; Wang, S.B.; Li, Z.; Wang, L.; Zhang, X.W. Cu₂O film via hydrothermal redox approach: Morphology and photocatalytic performance. *J. Phys. Chem. C* **2014**, *118*, 16335–16343. [[CrossRef](#)]
18. Ghodselahi, T.; Vesaghi, M.; Shafiekhani, A.; Baghizadeh, A.; Lameii, M. XPS study of the Cu@Cu₂O core-shell nanoparticles. *Appl. Surf. Sci.* **2008**, *255*, 2730–2734. [[CrossRef](#)]
19. Xu, H.; Wang, W.; Zhu, W. Shape Evolution and Size-Controllable Synthesis of Cu₂O Octahedra and Their Morphology-Dependent Photocatalytic Properties. *J. Phys. Chem. B* **2006**, *110*, 13829–13834. [[CrossRef](#)] [[PubMed](#)]
20. Wu, L.; Tsui, L.-K.; Swami, N.; Zangari, G. Photoelectrochemical Stability of Electrodeposited Cu₂O Films. *J. Phys. Chem. C* **2010**, *114*, 11551–11556. [[CrossRef](#)]
21. Wang, H.; Fan, W.; Xue, F.; Wang, X.; Li, X.; Guo, L. Chronic effects of six micro/nano-Cu₂O crystals with different structures and shapes on *Daphnia magna*. *Environ. Pollut.* **2015**, *203*, 60–68. [[CrossRef](#)] [[PubMed](#)]
22. Sedighi, A.; Montazer, M.; Samadi, N. Synthesis of nano Cu₂O on cotton: Morphological, physical, biological and optical sensing characterizations. *Carbohydr. Polym.* **2014**, *110*, 489–498. [[CrossRef](#)] [[PubMed](#)]
23. Yu, X.J.; Kou, S.; Zhang, J.; Tang, X.Y.; Yang, Q.; Yao, B.H. Preparation and characterization of Cu₂O nano-particles and their photocatalytic degradation of fluroxypyr. *Environ. Technol.* **2018**, *39*, 2967–2976. [[CrossRef](#)] [[PubMed](#)]
24. Tang, H.; Liu, X.; Xiao, M.; Huang, Z.; Tan, X. Effect of particle size and morphology on surface thermodynamics and photocatalytic thermodynamics of nano-Cu₂O. *J. Environ. Chem. Eng.* **2017**, *5*, 4447–4453. [[CrossRef](#)]
25. Liu, J.; Wang, S.; Wang, Q.; Geng, B. Microwave chemical route to self-assembled quasi-spherical Cu₂O microarchitectures and their gas-sensing properties. *Sens. Actuators B Chem.* **2009**, *143*, 253–260. [[CrossRef](#)]
26. Liu, X.Y.; Hu, R.Z.; Xiong, S.L.; Liu, Y.K.; Chai, L.L.; Bao, K.Y.; Qian, Y.T. Well-aligned Cu₂O nanowire arrays prepared by an ethylene glycol-reduced process. *Mater. Chem. Phys.* **2009**, *114*, 213–216. [[CrossRef](#)]
27. Jing, S.; Xing, S.; Wu, Y.; Wang, Y.; Zhao, B.; Zhao, C. Synthesis of octahedral Cu₂O microcrystals assisted with mixed cationic/anionic surfactants. *Mater. Lett.* **2007**, *61*, 2281–2283. [[CrossRef](#)]
28. Zhang, D.M.; Hu, B.S.; Guan, D.J.; Luo, Z.T. Essential roles of defects in pure graphene/Cu₂O photocatalyst. *Catal. Commun.* **2016**, *76*, 7–12. [[CrossRef](#)]
29. Wang, S.; Tang, Y.; Schobert, H.H.; Guo, Y.; Gao, W.; Lu, X. FTIR and simultaneous TG/MS/FTIR study of Late Permian coals from Southern China. *J. Anal. Appl. Pyrolysis* **2013**, *100*, 75–80. [[CrossRef](#)]
30. Liu, Z.; Li, J.; Zhao, X.; Li, Z.; Li, Q. Surface Coating for Flame Retardancy and Pyrolysis Behavior of Polyester Fabric Based on Calcium Alginate Nanocomposites. *Nanomaterials* **2018**, *8*, 875. [[CrossRef](#)]
31. Liu, Z.; Li, Z.; Zhao, X.; Zhang, L.; Li, Q. Highly Efficient flame retardant Hybrid Composites Based on Calcium Alginate/Nano-Calcium Borate. *Polymers* **2018**, *10*, 625. [[CrossRef](#)] [[PubMed](#)]
32. Zhao, W.; Qi, Y.; Wang, Y.; Xue, Y.; Xu, P.; Li, Z.; Li, Q. Morphology and Thermal Properties of Calcium Alginate/Reduced Graphene Oxide Composites. *Polymers* **2018**, *10*, 990. [[CrossRef](#)] [[PubMed](#)]
33. Sierra-Ávila, R.; Cadenas-Pliego, G.; Ávila-Orta, C.; Jiménez-Regalado, E.; Hernández-Hernández, E.; Jiménez-Barrera, R.M.; Pérez-Alvarez, M.; Padilla, V.C.; Camacho, O.P. Synthesis of Copper Nanoparticles Using Mixture of Allylamine and Polyallylamine. *J. Nanomater.* **2015**, *2015*, 140. [[CrossRef](#)]
34. Sierra-Ávila, R.; Cadenas-Pliego, G.; Ávila-Orta, C.A.; Betancourt-Galindo, R.; Jiménez-Regalado, E.; Jiménez-Barrera, R.M.; Pérez-Alvarez, M.; Martínez-Colunga, J.G. Synthesis of Copper Nanoparticles Coated with Nitrogen Ligands. *J. Nanomater.* **2014**, *2014*, 74. [[CrossRef](#)]
35. Jardón-Maximino, N.; Pérez-Alvarez, M.; Sierra-Ávila, R.; Ávila-Orta, C.A.; Jiménez-Regalado, E.; Bello, A.M.; González-Morones, P.; Cadenas-Pliego, G. Oxidation of Copper Nanoparticles Protected with Different Coatings and Stored under Ambient Conditions. *J. Nanomater.* **2018**, *2018*, 9512768. [[CrossRef](#)]
36. Li, J.; Li, Z.C.; Zhao, X.H.; Deng, Y.J.; Xue, Y.; Li, Q. Flame retardancy and thermal degradation mechanism of calcium alginate/CaCO₃ composites prepared via in situ method. *J. Therm. Anal. Calorim.* **2018**, *131*, 2167–2177. [[CrossRef](#)]
37. Ma, X.; Li, R.; Zhao, X.; Ji, Q.; Xing, Y.; Sunarso, J.; Xia, Y. Biopolymer composite fibres composed of calcium alginate reinforced with nanocrystalline cellulose. *Compos. Part A Appl. Sci. Manuf.* **2017**, *96*, 155–163. [[CrossRef](#)]

38. Laoutid, F.; Bonnaud, L.; Alexandre, M.; Lopez-Cuesta, J.-M.; Dubois, P.; Dubois, P. New prospects in flame retardant polymer materials: From fundamentals to nanocomposites. *Mater. Sci. Eng. R Rep.* **2009**, *63*, 100–125. [[CrossRef](#)]
39. Zhu, J.; Uhl, F.M.; Morgan, A.B.; Wilkie, C.A. Studies on the Mechanism by Which the Formation of Nanocomposites Enhances Thermal Stability. *Chem. Mater.* **2001**, *13*, 4649–4654. [[CrossRef](#)]
40. Chen, H.-B.; Shen, P.; Chen, M.; Schiraldi, D.A.; Zhao, H.-B. Highly efficient flame retardant polyurethane foam with alginate/clay aerogel coating. *ACS Appl. Mater. Interfaces* **2016**, *8*, 32557–32564. [[CrossRef](#)]
41. Tian, G.; Ji, Q.; Xu, D.; Tan, L.; Quan, F.; Xia, Y. The effect of zinc ion content on flame retardance and thermal degradation of alginate fibers. *Fibers Polym.* **2013**, *14*, 767–771. [[CrossRef](#)]
42. Liu, Y.; Zhang, C.-J.; Zhao, J.-C.; Guo, Y.; Zhu, P.; Wang, D.-Y. Bio-based barium alginate film: Preparation, flame retardancy and thermal degradation behavior. *Carbohydr. Polym.* **2016**, *139*, 106–114. [[CrossRef](#)]
43. Zhang, C.-J.; Liu, Y.; Cui, L.; Yan, C.; Zhu, P. Bio-based calcium alginate nonwoven fabrics: Flame retardant and thermal degradation properties. *J. Anal. Appl. Pyrolysis* **2016**, *122*, 13–23. [[CrossRef](#)]
44. Wang, Y.; Li, Z.; Li, Y.; Wang, J.; Liu, X.; Song, T.; Yang, X.; Hao, J. Spray-Drying-Assisted Layer-by-Layer Assembly of Alginate, 3-Aminopropyltriethoxysilane, and Magnesium Hydroxide Flame Retardant and Its Catalytic Graphitization in Ethylene–Vinyl Acetate Resin. *ACS Appl. Mater. Interfaces* **2018**, *10*, 10490–10500. [[CrossRef](#)]
45. Liu, Y.; Li, Z.; Wang, J.; Zhu, P.; Zhao, J.; Zhang, C.; Guo, Y.; Jin, X. Thermal degradation and pyrolysis behavior of aluminum alginate investigated by TG-FTIR-MS and Py-GC-MS. *Polym. Degrad. Stab.* **2015**, *118*, 59–68. [[CrossRef](#)]
46. Taghiyari, H.R. Fire-retarding properties of nano-silver in solid woods. *Wood Sci. Technol.* **2012**, *46*, 939–952. [[CrossRef](#)]



© 2019 by the authors. Licensee MDPI, Basel, Switzerland. This article is an open access article distributed under the terms and conditions of the Creative Commons Attribution (CC BY) license (<http://creativecommons.org/licenses/by/4.0/>).